






Article

Effects of Physically Adsorbed and Chemically Immobilized RGD on Cell Adhesion to a Hydroxyapatite Surface

Melissa Leitão¹, Elena Mavropoulos¹, Marcia Soares Sader², Andrea Costa¹ , Elvis Lopez¹,
Giselle Nogueira Fontes³, José Mauro Granjeiro³ , Tea Romasco^{4,5,*} , Natalia Di Pietro⁵ , Adriano Piattelli⁶,
Carlos Fernando Mourão⁴ , Gutemberg Gomes Alves⁷ and Alexandre Malta Rossi¹

- ¹ Coordenação de Matéria Condensada, Física Aplicada e Nanociência (COMAN), Centro Brasileiro de Pesquisas Físicas (CBPF), Rio de Janeiro 22290-180, Brazil; melgga@yahoo.com.br (M.L.); elena@cbpf.br (E.M.); andreamc@cbpf.br (A.C.); lopmezel@gmail.com (E.L.); rossi@cbpf.br (A.M.R.)
- ² Metallurgical and Materials Engineering, Federal University of Rio de Janeiro (UFRJ), Rio de Janeiro 21945-970, Brazil; marciasader@gmail.com
- ³ Brazilian National Institute of Metrology, Standardization and Industrial Quality, Rio de Janeiro 20261-232, Brazil; gisellefontes@gmail.com (G.N.F.); jmgranjeiro@inmetro.gov.br (J.M.G.)
- ⁴ Department of Clinical and Translational Research, Tufts University School of Dental Medicine, Boston, MA 02111, USA; carlos.mourao@tufts.edu
- ⁵ Department of Medical, Oral and Biotechnological Sciences, Center for Advanced Studies and Technology (CAST), “G. d’Annunzio” University of Chieti-Pescara, 66100 Chieti, Italy; natalia.dipietro@unich.it
- ⁶ School of Dentistry, Saint Camillus International University of Health and Medical Sciences, 00131 Rome, Italy; apiattelli51@gmail.com
- ⁷ Cell and Molecular Biology Department, Institute of Biology, Fluminense Federal University, Niteroi 24220-900, Brazil; gutemberg.alves@id.uff.br
- * Correspondence: tea.romasco@unich.it



Citation: Leitão, M.; Mavropoulos, E.; Sader, M.S.; Costa, A.; Lopez, E.; Fontes, G.N.; Granjeiro, J.M.; Romasco, T.; Di Pietro, N.; Piattelli, A.; et al. Effects of Physically Adsorbed and Chemically Immobilized RGD on Cell Adhesion to a Hydroxyapatite Surface. *Appl. Sci.* **2024**, *14*, 7479. <https://doi.org/10.3390/app14177479>

Academic Editor: Mary Anne Melo

Received: 30 July 2024

Revised: 18 August 2024

Accepted: 21 August 2024

Published: 23 August 2024



Copyright: © 2024 by the authors. Licensee MDPI, Basel, Switzerland. This article is an open access article distributed under the terms and conditions of the Creative Commons Attribution (CC BY) license (<https://creativecommons.org/licenses/by/4.0/>).

Abstract: The strategies used to associate peptide arginylglycylaspartic acid (RGD) with calcium phosphate grafts to enhance cell–biomaterial interactions have been controversial in the literature. Several works have demonstrated that RGD-functionalized hydroxyapatite (HA) surfaces improve cell adhesion, whereas others claim that RGD-loaded HA has an inhibitory effect when serum is present in the biological medium. To investigate such contradictory results, we associated RGD with the HA surface using physical adsorption and chemical bonding methods and evaluated the cell adhesion and spreading in pre-osteoblasts culture with and without fetal bovine serum (FBS). The effect of functionalization methods on the physicochemical characteristics of both surfaces was analyzed using multiscale techniques. Adsorption assays of serum allowed us to estimate the impact of the association method on the HA surface’s reactivity. Physically adsorbed RGD did not increase the number of adhered cells due to the weak interactions between the peptide and the surface. Although chemical binding stabilizes RGD on the HA, the functionalization procedure covered the surface with molecules such as (3-aminopropyl)triethoxysilane (APTEs) and carbodiimide, changing the surface’s chemical activity. Serum protein adsorption decreased by 90%, revealing a significant reduction in the surface interactions with molecules of the biological medium. The present study’s findings showed that the RGD’s physical association with HA did not improve cell adhesion and that this phenomenon is highly dependent on the presence of serum proteins.

Keywords: arginylglycylaspartic acid; immobilization; surface functionalization; hydroxyapatite; APTEs; FBS; cell adhesion

1. Introduction

New designs of biomaterials based on the association of peptides and proteins with hydroxyapatite (HA, $\text{Ca}_{10}(\text{PO}_4)_6(\text{OH})_2$) have been considered to increase osteoconductivity and promote bone tissue regeneration [1]. Although HA is biocompatible and bioactive,

its surface chemistry does not favor chemical binding to specific biological terminals in proteins/enzymes [2]. In general, interactions between proteins and HA surfaces occur according to electrostatic interactions [3]. In some cases, a surface interaction may induce inactivation by conformational changes, leading to protein denaturation or non-exposure of the site of interest at the time of adsorption [4]. Different approaches seek a more controlled interaction between cells and biomaterials, associating material surfaces with essential proteins and adhesion peptides, such as tripeptide RGD (arginylglycylaspartic acid, Arg-Gly-Asp), aiming at the obtention of innovative biomaterials for osteointegration [5,6].

RGD was discovered in the early 1980s as one of the cell adhesion motifs common to several matrix proteins, such as fibronectin (FN), vitronectin (VN), and bone sialoprotein (BSP) [7]. Since then, the idea of associating RGD as an isolated peptide segment into several biomaterials to increase cell adhesion and tissue growth has increased. Other derivative peptide segments were also developed, presenting linear or cyclic longer chains that still have the RGD sequence in their structure, such as VNRGD, FNRGD, GRGDSP, cycloRGD, and others, which are often called “RGD” or “segments containing RGD” [8,9].

The most used methods for RGD immobilization onto calcium phosphate surfaces involve physical adsorption or covalent bonds [10]. The latter occurs by introducing functional groups on the biomaterial surface, such as the alkyl, amino, and carboxyl groups, conducted using activated plasma, sputtering, or chemical reactions using additives, such as the silanizing agent (3-aminopropyl)triethoxysilane (APTES) [11].

Although the specific interaction of RGD segments with cell integrins is well known, there is controversy regarding the efficiency of RGDs in promoting cell adhesion when the peptide is associated with the HA surface. In vitro studies have indicated that the RGD/HA association may increase the number of adhered cells, even suggesting osteogenesis [10,12], while other authors have not observed such effects [13–15]. Previous studies have observed the increased adhesion of cells cultured in a serum-supplemented medium onto HA surfaces covalently bound to the peptide [16,17]. Furthermore, Sawyer et al. [18], who physically adsorbed the peptide onto an HA surface, observed increased cell adhesion and spreading, although smaller than the surface covered with fetal bovine serum (FBS). Hennessy et al. [14], on the other hand, observed the inhibition of cell adhesion, suggesting that the differences in the biological response to HA/RGD associations may depend on the peptide’s physicochemical interaction with the biomaterial surface, which, in turn, may be affected by the choice of immobilization method. Both studies claimed that serum proteins could compete for the HA binding sites, thus displacing the weakly bound peptides onto the surface, possibly triggering an anoikis apoptotic pathway.

These results have led to the hypothesis that the differences in the biological response to RGD/HA associations may depend on the peptide’s physicochemical interaction with the biomaterial surface, which, in turn, may be affected by the choice of immobilization method. However, this hypothesis remained untested since most cell/surface interaction studies employed RGD immobilized through physical adsorption, and there is no direct evidence in the literature comparing the two methods on cell adhesion effects in the presence or absence of serum proteins. In this context, this work aimed to understand the interactions of RGD with HA surfaces by comparing its functionalization through physical adsorption and chemical immobilization, its impacts on interaction with serum proteins, and the adhesion of pre-osteoblasts in vitro.

2. Materials and Methods

2.1. Synthesis and Sample Preparation

All reagents were obtained from Sigma-Aldrich (St. Louis, MO, USA) and were of the highest purity available. HA was synthesized via the wet method with a molar ratio of Ca/P = 1.67, as described elsewhere [19]. Briefly, HA was synthesized by the dropwise addition of an aqueous 0.12 M $(\text{NH}_4)_2\text{HPO}_4$ solution to an aqueous solution of 0.2 M $\text{Ca}(\text{NO}_3)_2$, with pH = 9 at 90 °C. After the addition, the resulting suspension was aged for 3 h. The solid was then filtered, washed three times, and dried at 80 °C. The dried

aqueous solution at room temperature for 6 h using intense agitation and washed three times with ultrapure water. The HA samples were reacted overnight with a 100 µg/mL RGD aqueous solution. As described above, the c-RGD/HA samples were then sonicated for 5 min at room temperature to remove the weakly bound RGD peptides. The aqueous solutions used in the experiments were sterilized using Sigma-Millipore membranes (0.22 µm, Sigma-Aldrich, St. Louis, MO, USA). Table 1 summarizes the sample designation, composition, and solutions used at each immobilization stage. Immobilization using RGD-FITC (ChemPep Inc., Wellington, FL, USA) occurred in the same manner as described in the third step of the immobilization.

Table 1. Treatments and experimental groups of the study.

Samples	Material	Treatment Solutions
HA ¹	HA	untreated
Physical immobilization p-RGD/HA	HA + RGD	100 µg/mL (RGD)
Chemical immobilization		
c-HA1	HA + APTES ²	20 mM (HA disc); 40 mM (HA powder) (APTES)
c-HA2	HA + APTES + EDC ³	0.3% EDC
c-RGD/HA	HA + APTES + EDC + RGD	100 µg/mL (RGD)

¹ Hydroxyapatite; ² (3-aminopropyl)triethoxysilane; ³ 1-ethyl-3-(3-dimethylaminopropyl) carbodiimide.

2.3. Physicochemical Characterization

2.3.1. Chemical and Structural Characterization of HA

The HA powder was characterized by X-ray diffraction using HZG4 (Carl Zeiss, Oberkochen, Germany) with CuK α radiation ($\lambda = 1.5418 \text{ \AA}$), θ — 2θ varying between 10 and 100°, and a step of 0.05 °/s. For the HA discs, the grazing-incidence X-ray diffraction technique (GIXRD) was used, with a fixed incident angle $\theta = 0.5^\circ$, 2θ detector in the range of 10–60°, and a step of 0.04 °/s.

The Fourier-transform infrared spectroscopy (FTIR) spectrum of the HA powder was collected by a IR-Prestige-21 / AIM-880 spectrophotometer (Shimadzu Scientific Instruments, Riverwood Drive Columbia, MD, USA), over a range of 4000–400 cm^{-1} , with a resolution of 4 cm^{-1} and 500 scans using KBr pellets (Shimadzu Scientific Instruments, Riverwood Drive Columbia, MD, USA). The HA discs were analyzed via Attenuated Total Reflectance (ATR) using an AIM-880 Microscope (FTIR/ATR, Shimadzu Scientific Instruments, Riverwood Drive Columbia, MD, USA), coupled to an IR-Prestige-21, using a range of 4000–750 cm^{-1} , with a resolution of 4.0 cm^{-1} . Three areas in different sample regions were analyzed using 200 scans/region. The spectra were analyzed by IR-solution software version 1.60 when using an atmosphere correction.

Elemental analyses of Ca and P were carried out using an X-ray Fluorescence (XRF) Spectrometer (Axios mAX, Malvern Panalytical, Malvern, UK) operating at 40 kV and 50 mA with a Ge (111) crystal, a collimator of 550 µm, and a flow detector for the K α lines of Ca and P.

2.3.2. Zeta Potential

Zeta potential (ZP) measurements of the sample dispersion were performed before and after each step of the surface immobilization using 10 mg of the HA powder in 15 mL of a 1 mM potassium chloride (KCl) solution. The measurements were obtained by varying the pH of the dispersing solution in the range of 3–11, using a 0.05 M sodium hydroxide (NaOH) solution and 0.05 M hydrochloric acid (HCl) and analyzed on Zetasizer Nano ZS equipment with MPT-2 (Malvern Panalytical, Malvern, UK).

2.3.3. Contact Angle

The contact angle was measured using a Advanced Goniometer/500-F1 (Rame-Hart, Randolph, NJ, USA). Two drops of ultrapure water (200 μ L) were released on the HA disc (5 discs per sample group); 30 measures were performed with a time interval of 0.2 s, and the results were captured by DROP image Advanced software version 2.7.

2.3.4. Fluorescence Microscopy and Microplate Reader

An inverted fluorescence microscope (Axio Observer A1, Zeiss, Germany) captured the surface images with 5 \times magnification of the p-RGD-FITC/HA and c-RGD-FITC/HA discs (3 images of each sample, n = 2 per group). Zen2-ProPlus 6.0 software analyzed the fluorescence emission intensity of each disc, with and without RGD.

A fluorimeter microplate reader (Synergy II, BioTek Instruments, Winooski, VT, USA) quantified the fluorescence of the immobilized RGD-FITC on the p-RGD/HA and the c-RGD/HA samples at an absorbance of 590 nm. Three independent experiments were conducted (n = 5) for each sample group. Before the measurements, the discs were washed carefully and extensively with ultrapure water until the supernatant fluorescence was near zero. Afterward, the dried discs were submitted to both analyses.

2.3.5. X-ray Photoelectron Spectroscopy (XPS)

The chemical surface analyses on the HA discs were performed by X-ray photoelectron spectroscopy (XPS) measurements when using a PHOIBOS 100/150 spectrometer (SPECS Group, Berlin, Germany), with a hemispheric analyzer operating at 1486.6 eV of Al K α . The spectra were collected with a high-resolution polychromatic X-ray source, with an energy step of 0.02 eV. CasaXPS Processing Software version 2.3.26 was used to adjust the peak positions of the Ca 2p, P 2p, O 1s, C 1s, and N 1s levels and determine the chemical binding energies (BEs) of some of the species formed, as well as to calculate the relative atomic quantities of the samples. The spectra were calibrated using adventitious carbon at C1s = 284.5 eV. The differences in the 2p_{3/2} and 2p_{1/2} levels for P, Ca, and Si were $\Delta P(2p_{3/2}-2p_{1/2}) = 0.84$ eV, $\Delta Ca(2p_{3/2}-2p_{1/2}) = 3.55$ eV, and $\Delta P(2p_{3/2}-2p_{1/2}) = 0.86$ eV, respectively [20].

2.4. Cell Adhesion

MC3T3-E1 pre-osteoblastic cells (ATCC 7594, BCRJ, Rio de Janeiro, RJ, Brazil) were used to evaluate the cellular responses to the different disc surfaces. The cells were routinely cultured with 5% CO₂ at 37 °C on α -Minimum Essential Medium (α -MEM, Sigma, USA) supplemented with 10% FBS (Gibco™, Thermo Fisher Scientific, Boston, MA, USA). The MC3T3-E1 cells (density of 2.0 \times 10³) were seeded over the HA, c-RGD/HA, and p-RGD/HA samples and incubated for 24 h in α -MEM, with and without 10% FBS. After this period, the samples were fixed in 4% paraformaldehyde (PFA) at room temperature. The cells were washed with phosphate-buffered saline (PBS) pH = 7.4, permeabilized with 0.1% Triton X-100, stained with Rhodamine-Phalloidin (Alexa Fluor® 546, Life Technologies, Thermo Fisher Scientific, Boston, MA, USA) for 30 min, and mounted on glass slides containing DAPI/DABCO™ (Fluoroshield™, Sigma-Aldrich, St. Louis, MO, USA). The images were taken using an Axio Observer A1 inverted fluorescence microscope (Zeiss, Germany). The cell numbers and the cytoplasmic spreading area were quantified using 10 images per sample with Image-Pro Plus 6.0 (IPP6) software. Three experiments were performed, resulting in 30 images per sample.

For qualitative evaluation via scanning electron microscopy (SEM), the samples were fixed in Karnovsky's solution, washed in a cacodylate buffer, and postfixed in 1% osmium tetroxide (Sigma-Aldrich, St. Louis, MO, USA). After three washes with the cacodylate buffer, the samples were dehydrated in increasing concentrations of ethanol (30, 50, 70, 90, and 100%), critical point dried, coated with gold, and observed at 15 kV, with secondary electron imaging by SEM (TESCAN VEGA3, TESCAN, Brno, Czechia) for the cell morphology evaluation.

2.5. Fetal Bovine Serum (FBS) Adsorption on the HA, c-RGD/HA, and p-RGD/HA Discs

The HA, p-RGD/HA, and c-RGD/HA discs were immersed in 1000 μL of a 10% FBS (Gibco™, Thermo Fisher Scientific, Boston, MA, USA) aqueous solution for 3 h at room temperature. Afterward, the samples were washed gently in ultrapure water and dried naturally; the control sample from each group was exposed only to ultrapure water. All samples were immersed in 500 μL of a 1.5% sodium dodecyl sulfate (SDS, Sigma-Aldrich, St. Louis, MO, USA) aqueous solution for 3 h. The supernatant was collected and read on a NanoDrop Spectrophotometer (NanoDrop 2000c, Thermo Fisher Scientific, Boston, MA, USA) at a wavelength of 280 nm. Every assay was performed in quintuplicates.

2.6. Statistical Analysis

All the data were expressed using the arithmetic mean \pm standard error of the mean. The Shapiro–Wilk test verified the normality of the data. The analyses of variance were performed for the cell adhesion assay using the Kruskal–Wallis Test, Dunn’s Post Hoc Test (comparing all of the groups), and One-Way ANOVA, with Tukey’s Post Hoc Test used for the FITC-RGD detection. The contact angle and the adsorbed FBS used One-Way ANOVA, with Tukey’s multiple comparisons test. Statistical significance was considered with an alpha error of 5%. All data analyses used GraphPad Prism 7 (San Diego, CA, USA) software.

3. Results

3.1. Physicochemical Evaluation

The X-ray diffraction (XRD) and GIXRD patterns of the HA powder and disc displayed characteristic peaks of the high crystalline HA phase (JCPDS-00-009-0432) (Figure 2).

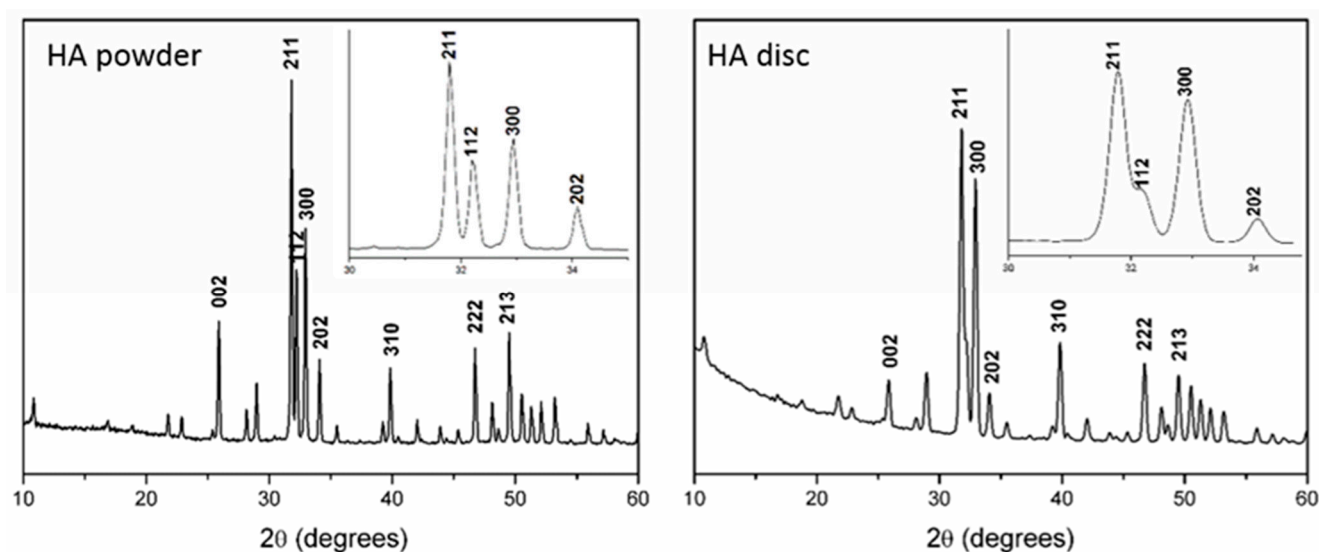


Figure 2. X-ray diffraction (XRD) patterns of the HA powder and the grazing-incidence X-ray diffraction (GIXRD) of the discs after the heat treatment and RGD functionalization.

The change in the relative intensities of the 002, 211, and 300 peaks of the GIXRD pattern was attributed to surface stress caused by disc pressing, followed by sintering. Chemical analysis and the FTIR spectra confirmed the hydroxyapatite chemical composition. The HA powder displayed a calcium phosphate ratio of 1.68, and the FTIR spectrum consisted of $(\text{PO}_4)^{3-}$ bands at 1091 cm^{-1} (v3a), 1044 cm^{-1} (v3b), 959 cm^{-1} (v1), 601 cm^{-1} (v4), and 569 cm^{-1} (v4), with OH- bands at 3570 cm^{-1} and 632 cm^{-1} . The complete results from the Chemical analyses by XRF and FTIR are presented in Table S1 (Supplementary Materials) and Figure S1 (Supplementary Materials), respectively.

The ZP of the HA powder nanoparticles immersed in sodium chloride (NaCl) solutions was assessed at pH values of between 3 and 11 before and after RGD immobilization. Two

APTES molarities (20 and 40 mM) were analyzed for the silanization step. However, due to the distinct surface areas, we continued with 40 mM to treat HA powders and 20 mM to treat HA discs. It was found that the untreated HA surface displayed a ZP of -20.6 ± 1.7 mV at pH = 7.0 and an isoelectric point (IP) of 4.99 (Table 2).

Table 2. Surface charge analysis of samples before and after RGD physical and chemical immobilization steps using the Zeta Potential (ZP) and Contact Angle (CA) technique.

Samples	IP ¹	pH ²	ZP (mV)	Groups ³	CA (°) ⁴
HA	4.99 (± 0.01)	7.0 (± 0.5)	$-20.6 (\pm 1.7)$	OH ⁻ and PO ₄ ⁻	61 (± 2)
p-RGD/HA	6.76 (± 0.06)	7.7 (± 0.3)	1.0 (± 1.9)	COOH ⁻ and NH ₂ ⁺	91 (± 1)
p-RGD/HA *	5.91 (± 0.04)	7.1 (± 0.0)	$-5.5 (\pm 0.6)$	COOH ⁻	83 (± 2)
c-HA1	10.05 (± 0.03)	7.9 (± 0.4)	10.6 (± 1.3)	NH ₂ ⁺	75 (± 1)
c-HA2	8.24 (± 0.06)	7.9 (± 0.4)	2.1 (± 0.9)	NH ₂ ⁺ and CH ³⁻	68 (± 3)
c-RGD/HA	5.35 (± 0.03)	7.4 (± 0.3)	$-5.7 (\pm 0.6)$	COOH ⁻	69 (± 4)
c-RGD/HA *	5.34 (± 0.05)	7.1 (± 0.1)	$-4.9 (\pm 0.6)$	COOH ⁻	67 (± 2)

¹ The isoelectric point (IP) values of each sample demonstrate the modification of the HA surface charge during the immobilization steps; ² pH values of samples dispersed in potassium chloride (KCl) solutions at the moment of the ZP measurements; the mean value of 3 replicates (\pm standard deviation); ³ possible functional groups exposed on the HA surface at each stage. However, the overlapping of films does not occur totally and homogeneously; ⁴ CA values using dripping water; the mean value of 5 replicates (\pm standard deviation). * Sample evaluated after sonication.

After the RGD physical adsorption, the IP of p-RGD/HA increased to 6.76, with a ZP of $+1.0 \pm 1.9$ mV at pH = 7.7, confirming the RGD bond to the HA surface. Removing the weakly immobilized RGD peptides through sonication did not significantly change p-RGD/HA's IP (Table 2).

In the group submitted to chemical immobilization, the samples that were silanized in the first stage (c-HA1) with 20mM showed a positive charge at pH = 4 ($+18.7 \pm 1.3$ mV) and $+2.3 \pm 0.5$ mV around pH = 7, considered low compared to the 40 mM sample, which presented a charge above +30 ($+43.8$) at pH 4 and $+10.6 \pm 1.3$ mV at pH = 7. In the subsequent stages, spacer (EDC and c-HA2) insertion and the immobilization of RGD (c-RGD/HA) markedly reduced the ZP to -5.7 mV in a 40 mM sample at pH around 7. The charges were not affected by sonication. During the first two steps of RGD chemical immobilization, the high IP values reflected the silanization process and the subsequent coating with EDC. By the end of the chemical RGD immobilization process, the IP value of 5.34 was close to the control (4.99) and similar to p-RGD/HA, indicating a surface with a negative charge.

Contact angle (CA) measurements were used to assess the effect of RGD on the wettability of each HA disc surface following either the physical or chemical addition of RGD, as summarized in Table 2. The untreated HA surface exhibited a CA of $61^\circ \pm 2$, indicating its expected hydrophilic nature. After RGD adsorption, the CA of the surface physically adsorbed with RGD (p-RGD/HA) immediately increased to $91^\circ \pm 1$ ($p < 0.05$), but it later decreased to $83^\circ \pm 2$ after sonication was performed to remove weakly bound peptides. Regarding the chemically bound RGD material (c-RGD/HA), the CA values varied significantly during its production steps, from $75^\circ \pm 1$ following the APTES treatment to $68^\circ \pm 3$ after the subsequent carbodiimide treatment, remaining at similar levels ($69^\circ \pm 4$) in the final step, where the RGD peptide was finally associated with the HA/APTES/Carbodiimide surface, resulting in a material with a wettability more similar to the untreated HA than p-RGD/HA.

The XPS spectra of the untreated sample consisted of binding energies for O 1s at 532.3, 530.7, and 528.6 eV; Ca 2p_{3/2} at 346.7.1 and 344.5 eV; P 2p_{3/2} at 132.5 eV; and C 1s at 288.3, 286.1, and 284.5 eV (Table 3).

The Ca/P ratio was 1.3, typical of a calcium-deficient HA surface. While the chemical treatments decreased the surface Ca and P ratio, as shown in Table 2, they did not modify the binding energies of Ca 2p, P 2p, O 1s, and C 1s (Table 3). Nitrogen atoms belonging to the RGD structure were detected in the RGD-coated samples (p-RGD/HA and c-RGD/HA),

indicating the presence of the peptide. The N/Ca ratio was around 0.06 for the p-RGD/HA and c-RGD/HA samples. This result has suggested that less than one N atom was linked per HA unit cell on the disc surface.

Table 3. XPS atomic composition in percentages of elements present on HA surfaces and their ratios of N. The binding energies of the samples before and after treatment and their spectra are shown in Figure S2 (Supplementary Materials).

Samples	at. %						N/Si	N/Ca	Ca/P
	Ca 2p	P 2p	O 1s	C 1s	Si 2p	N 1s			
HA	21.7	16.7	47.5	14.2	-	-	-	-	1.3
p-RGD/HA	22.0	16.6	46.2	14.2	0.0	1.0	1.0	0.05	1.3
c-RGD/HA	20.9	15.9	44.8	15.8	1.2	1.4	1.2	0.07	1.3

The p-RGD/HA and c-RGD/HA discs (Figure 3A,B) displayed higher fluorescent intensity than the auto-fluorescence of HA (Figure 3C) that was present all over the discs (Figure 3A,B). Figure 3D shows that there was no significant difference between the fluorescence of p-RGD/HA and c-RGD/HA samples ($p > 0.05$), with the statistical difference with all other groups of $p < 0.0001$ (one-way ANOVA) (Figure 3D).

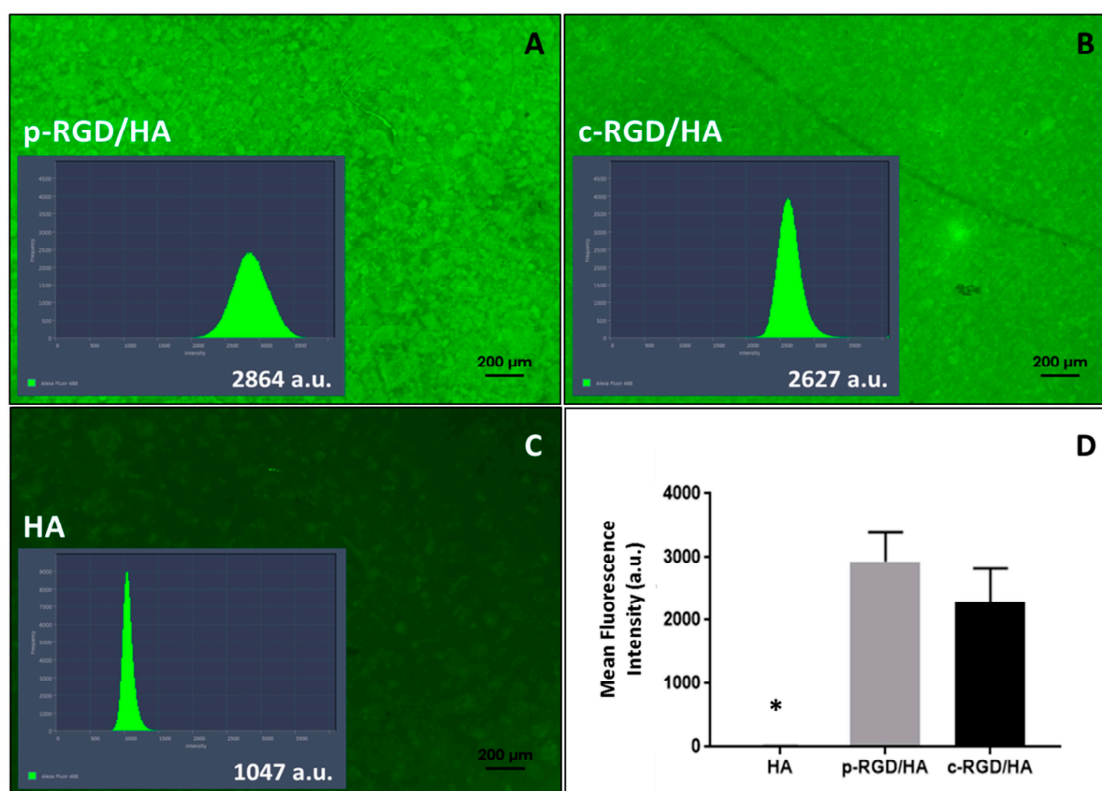


Figure 3. Fluorescence emission intensity of physically adsorbed RGD-FITC (p-RGD/HA) and chemically bound RGD-FITC (c-RGD/HA) on HA discs. (A,B) Images of the discs after one hour of reaction with RGD-FITC solution and their histograms of fluorescence intensity (a.u.: arbitrary unit) obtained and the fluorescence emission intensity quantified through software Image Zen2-ProPlus version 2 using the peak area of total fluorescence light. (C) The auto-fluorescence of HA control sample with an intensity of 1047 a.u. after remaining one hour in milli-Q water. (D) A graph of the average fluorescence intensity of the discs measured by a microplate reader; the result shows the average of 3 independent experiments carried out in triplicate. * Statistical difference to all other groups ($p < 0.0001$, one-way ANOVA).

The atomic force microscopy (AFM) images of HA disc samples, before and after RGD immobilization, were processed by NanoScope software version 1.40R2. The two-dimensional (2D, height, and peak force error) and three-dimensional (3D) topographic images presented in Figure 4 show the difference in surface morphology of the functionalized samples compared to the control as described in Table 4. The HA sample had an average surface roughness ($R_{rms}/9 \mu\text{m}^2$) of 20.7 nm. The increase in the average roughness of the intermediate step c-HA1 (25.2 nm) and c-HA2 (25.6 nm) samples and decrease in valley and peak amplitudes shows the superposition of the APTES and EDC films, proving the modification of the chemically treated surfaces. The samples with RGD, p-RGD/HA, and c-RGD/HA presented $R_{rms} = 27.6 \text{ nm}$ and 21.2 nm , respectively, showing the production and overlapping of the films, in addition to the morphological difference in the topography between them and both compared to the control. The cross-section of the 2D image shows the variation in the amplitude between peaks and valleys of the samples, visibly smaller in the c-RGD/HA sample.

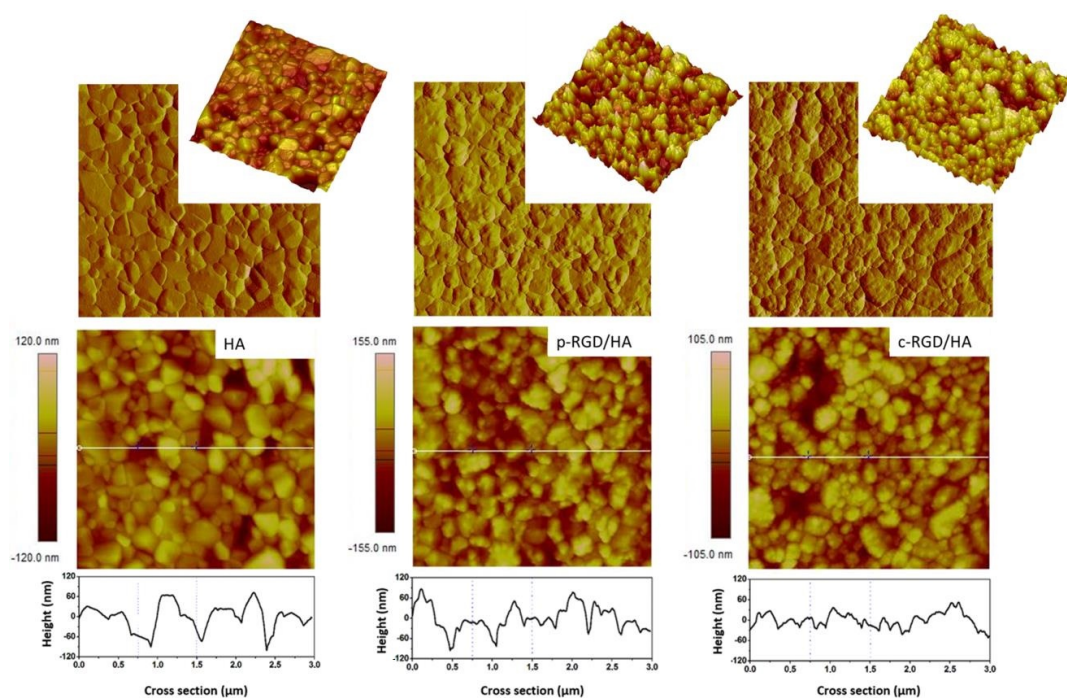


Figure 4. Surface morphology through two-dimensional (2D) and three-dimensional (3D) atomic force microscopy (AFM) topographic height images and their cross-sections showing the decrease in the amplitude between peaks and valleys in c-RGD/HA and the increase in p-RGD/HA with increase in average roughness (R_{rms}) in functionalized samples when compared to the HA control. $3.0 \mu\text{m} \times 3.0 \mu\text{m}$ images.

Table 4. Surface roughness (R_{rms}) of HA discs before and after RGD immobilization.

Sample	Description	Average Surface Roughness (R_{rms})	Key Observations
Control	HA (untreated)	20.7 nm	Baseline surface roughness, no modification.
c-HA1	HA + APTES (first chemical treatment)	25.2 nm	Increased roughness due to APTES film application.
c-HA2	HA + APTES + EDC (second chemical treatment)	25.6 nm	Slightly increased roughness due to additional EDC film application.
p-RGD/HA	HA with physically adsorbed RGD	27.6 nm	Highest roughness, indicating overlapping films and morphological changes.
c-RGD/HA	HA + APTES + EDC + RGD (chemically immobilized RGD)	21.2 nm	Decreased valley and peak amplitude, indicating smaller variations in topography.

3.2. Cell Adhesion Evaluation

The MC3T3-E1 cells cultured for 24 h in the FBS-free α -MEM medium did not adhere to the HA surface after successive dehydration washes during the sample processing for SEM (Figure 5).

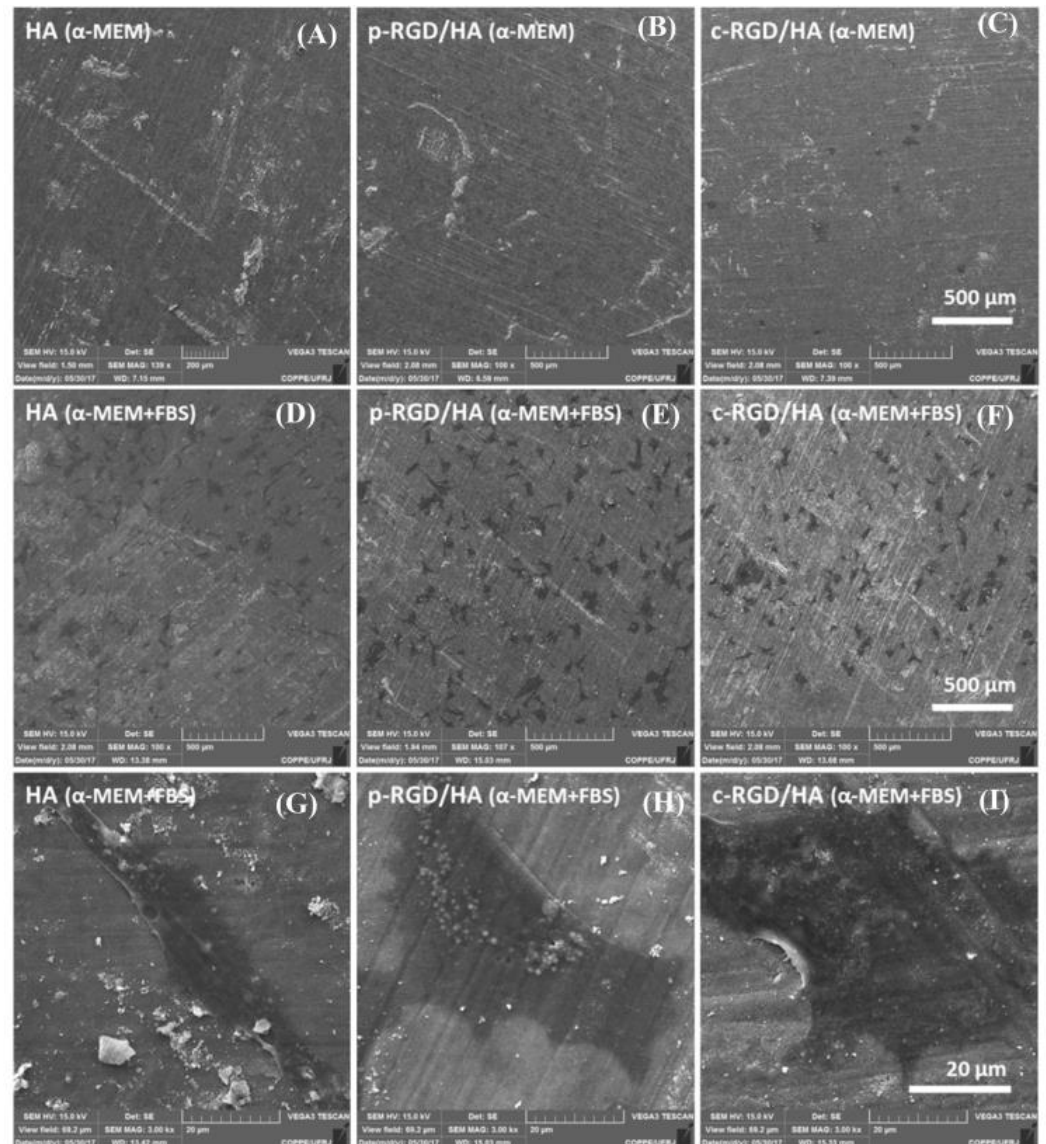


Figure 5. Scanning electron microscopy (SEM) of the MC3T3-E1 cell adhesion after 24 h on the HA (A), p-RGD/HA (B), and c-RGD/HA (C) surfaces when cultivated in an α -Minimum Essential Medium (α -MEM) medium free of fetal bovine serum (FBS) and α -MEM medium with FBS (D–F). Magnification: 100 \times . Under high magnification (3K), examples of cell morphological units found on the three HA surfaces (G–I) when cultivated in the presence of FBS. Asterisks and arrows indicate the presence of cells.

However, it was possible to observe some cells on the c-RGD/HA surface, indicating that RGD chemically binding on the HA surface allowed for the more stable adhesion of MC3T3-E1 when cultivated in a non-supplemented medium. When the cells were grown in a supplemented medium, no significant differences occurred in the cell adhesion among the functionalized samples. The elongated cells presented two to three anchorage points, and more widely spread lamellar shapes were found on all three HA surfaces.

Through fluorescence microscopy and biostatistics analysis (Figure 6), it was not possible to observe any significant difference in the number of cells adhered to c-RGD/HA, p-RGD/HA, or the control when cultivated in the medium without FBS (-FBS) (Figure 6A, white columns).

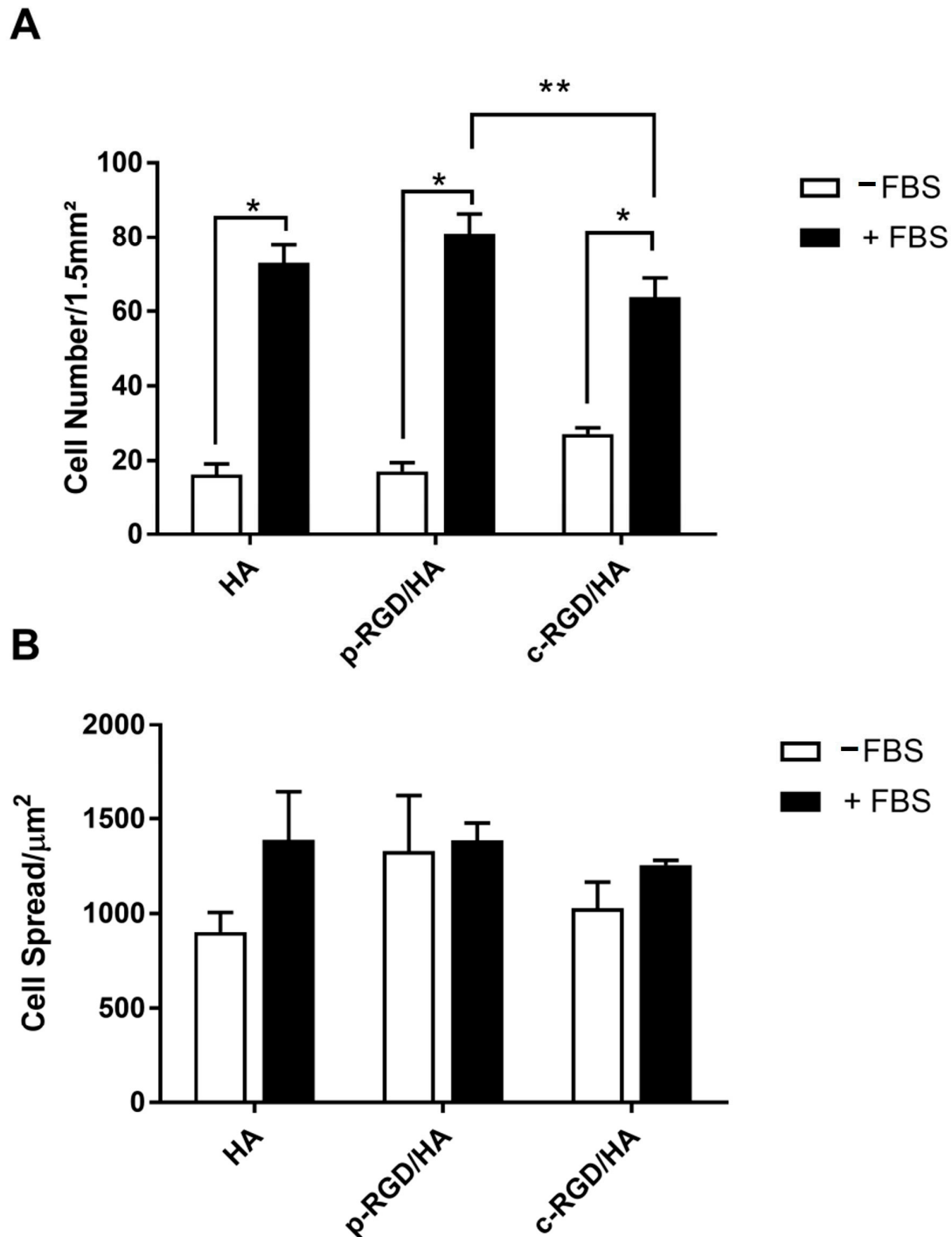


Figure 6. (A) Quantitative analysis of the MC3T3-E1 adhesion and (B) cell spreading after 24 h of cultivation on the functionalized HA surfaces in medium with and without FBS. The ratio between the area occupied by the cells and the total number of cells quantified per image was expressed by cell spreading data. The statistical analysis consisted of Two-way ANOVA, with Tukey's multiple comparisons test (** $p < 0.0001$ and * $p < 0.05$).

However, when compared with the supplemented group (+FBS), it was possible to notice a significant difference in the number of cells ($p < 0.0001$). The number of cells adhered in c-RGD/HA was significantly lower than that quantified in p-RGD/HA ($p = 0.0330$). There was no difference between p-RGD/HA and the control (Figure 6A, black columns). Regarding the sprawling area, there were no significant differences between all samples (Figure 6B).

The HA, p-RGD/HA, and c-RGD/HA discs were immersed in a 10% FBS aqueous solution to evaluate the samples' capacity to adsorb FBS proteins after 3 h of exposure. Figure 7 shows the surface-adsorbed proteins of FBS. However, HA and p-RGD/HA adsorbed $87.76 \pm 9.6 \mu\text{g/mL}$ and $74.93 \pm 7.2 \mu\text{g/mL}$, respectively, while c-RGD/HA adsorbed $11.36 \pm 2.0 \mu\text{g/mL}$, a significantly lower amount of FBS proteins when considering $* p < 0.0001$.

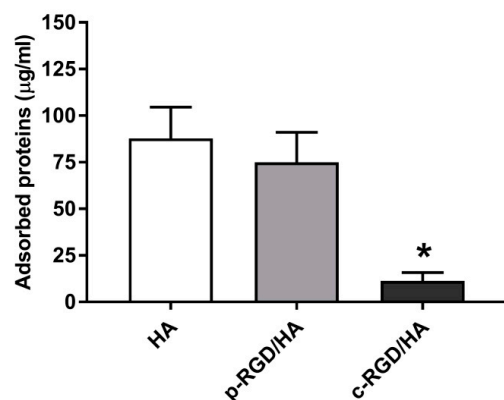


Figure 7. Quantitative analysis of the total FBS proteins adsorbed on the sample surfaces after 3 h of incubation in a 10% FBS solution. Afterward, the samples were washed gently in ultrapure water and reacted for 3 h in a 1.5% sodium dodecyl sulfate (SDS) solution. The collected supernatant was read on a Thermo Scientific™ NanoDrop 2000c Spectrophotometer at a wavelength of 280 nm. Statistical analyses were considered ($n = 5$) for each sample. The statistical analyses consisted of One-way ANOVA, with Tukey's multiple comparisons test ($* p < 0.0001$).

4. Discussion

The association of RGD with a hydroxyapatite surface has been proposed as a tool to improve the biological efficiency of osteoconductive scaffolds in a bone regeneration process [6]. Despite the numerous studies on the subject, there is still controversy regarding the biological effects of RGD/HA association. Non-convergent results from different studies may be attributed to differences between HA samples, the methods for immobilizing RGD on the HA surface, association with various types of RGD, cell culture using different cell types, and the use or not of a supplemented culture medium. This study aimed to address these inconsistencies by comparing the effects of physical adsorption and chemical immobilization of RGD on HA surfaces, focusing on their impacts on surface characteristics and cell adhesion in the presence or absence of serum proteins.

It is well-established that the physicochemical properties of HA, such as stoichiometry, crystallinity, surface chemistry, topography, wettability, and surface energy, play critical roles in mediating the interaction between RGD and the biomaterial surface, which in turn influences cellular responses [13]. The present study demonstrated that both immobilization methods alter the HA surface's physicochemical characteristics, with each method presenting distinct advantages and challenges. The chemical immobilization method, in particular, led to a more stable RGD attachment, but it also modified the surface properties in ways that could influence protein adsorption and cell interactions differently compared to physical adsorption.

The control of binding RGD to the surface is one of the main challenges for a reliable assessment of the role of RGD in cell adhesion. Many works use physical adsorption, which

links the peptide terminals of NH_3^+ and COO^- to the HA surface's negative and positive sites through electrostatic interactions. Interactions with proteins from biological fluids may break these weak bonds, releasing the surface's peptide [11,13]. In addition, there is no certainty that the RGD active site ($-\text{COO}^-$) would be available to interact with the cell ligands. Our findings suggest that while physical adsorption is simpler and maintains the HA surface's native properties to some extent, the weak interaction between RGD and HA limits the effectiveness of this method in promoting cell adhesion, particularly in the presence of competing serum proteins. Despite some studies showing that RGD adsorption promotes cell adhesion and spreading [16,17], Sawyer et al. [18] found that HA discs adsorbed with RGD promoted lower interactions with the mesenchymal cells than the same system after an overcoating with serum. The authors concluded that the interaction of serum proteins with the HA surface could neutralize the effect of adsorbed RGD on cell adhesion. This study corroborates these findings, demonstrating that the presence of serum proteins significantly influences the effectiveness of RGD-functionalized surfaces, with the chemically immobilized RGD showing a reduced protein adsorption capability, which could explain the lower cell adhesion observed in serum-supplemented conditions.

Some studies have used the chemical immobilization of RGD on the surface of HA [21,22]. This method ensures the peptide's stability on the surface, but it requires surface functionalization with chemical agents, such as APTES and carbodiimide. It is also necessary to ensure that the RGD carboxylic sites can interact with the cellular integrins. These chemical immobilization methods may lead to positive results regarding cell adhesion and spreading, as shown by Balasundaram et al. [22] and Durrieu et al. [21]. However, in both studies, the adhesion tests occurred under a supplemented medium (10% FBS and 5% bovine serum albumin, BSA, respectively). Furthermore, no work has compared the *in vitro* performance of these different RGD immobilization methods in the presence or absence of serum proteins. Our results extend this understanding by showing that while chemical immobilization stabilizes RGD on the HA surface, it also modifies the surface properties in ways that reduce serum protein adsorption, leading to a complex interplay between the surface's chemical stability and its biological activity in different culture conditions.

The present work used a nanocrystalline powder with $\text{Ca}/\text{P} = 1.68$ to analyze the changes in the HA surface after the RGD immobilization and test the efficiency of the physical and chemical methods used to immobilize RGD. XPS analyses showed that sample treatments to associate RGD physically or chemically to the HA surface changed the chemical composition and stoichiometry of the HA surface significantly, even though the Ca/P ratio was not affected by the treatments. The detection of nitrogen binding energy confirmed the RGD association with the HA surface in p-RGD/HA and c-RGD/HA samples. The N/Ca ratio was around 0.06 for both the p-RGD/HA and c-RGD/HA samples, suggesting that less than one N atom from the RGD molecule was linked per HA unit cell in both samples. The fluorescence assays using RGD-FITC confirmed similar amounts of RGD on p-RGD/HA, and c-RGD/HA also supported the XPS analysis that showed the expected Ca and P binding energies of the uncoated-HA [23], identifying the NH_x and N-C bonds that were associated with RGD [20]. Altogether, the presented results indicate that similar RGD amounts were immobilized onto the HA surface by the physical and chemical methods using free $-\text{COOH}$ sites, suggesting a similar efficiency for both methods, at least in the present experimental conditions.

However, the choice of immobilization method significantly influenced the surface topography and chemistry of the HA samples. Atomic force microscopy (AFM) revealed that chemically immobilized RGD (c-RGD/HA) produced a smoother surface compared to physically adsorbed RGD (p-RGD/HA), which displayed a higher average surface roughness. This difference in topography likely results from the more uniform coating achieved through chemical immobilization, which may reduce the exposure of HA's underlying structure. These surface topography and chemical composition modifications caused by the surface treatment on p-RGD/HA and c-RGD/HA samples also led to changes in surface

charge and surface wettability. ZP analysis assigned an IP of 4.99 to HA powder, assuring a high negative surface charge in the *in vitro* assays' conditions. After physical adsorption, the p-RGD/HA sample's IP increased to a value of 6.76, indicating that RGD is bound to the HA surface with the -N terminals that were likely exposed on the surface, thereby modifying the surface charge by the presence of RGD. In the first immobilization step, the APTES coating introduced amine (NH_2^+) radicals on the silanized HA c-HA1 sample surface [11], leading to an IP of 8.24 and a positive surface charge at neutral pH. After treatment with carbodiimide and RGD, the surface IP was markedly reduced to 5.35 due to the new layers rich in COO^- when introduced on the HA surfaces [10,11]. These results confirmed the significant difference in HA surface charge when RGD molecules are associated with the surface through physical or chemical bonds. It is important to highlight the relevance of removing the weakly bound peptides to obtain the functionalized surfaces, predominantly exposing the RGD -C terminus, which is directly involved in binding cellular integrins [24].

Moreover, the wettability of HA surfaces, as indicated by contact angle (CA) measurements, was altered by RGD immobilization. The surface hydrophilicity is an indicator of the potential of the calcium phosphate surface to interact with molecules and cells [25]. Functional groups, such as -OH, -CH₃, COOH, and NH₂, influenced the adsorption of the proteins on the calcium phosphate surfaces and, consequently, the protein–cell interactions. Moreover, the coatings of N⁺, O⁺, and Si⁺ ions reduce the surface's free energy. In general, it is well established that a hydrophilic character reduces the adsorption of the proteins and cell adhesion by providing low free interfacial energy [26]. However, adhesive proteins containing RGD, such as FN and VN, prefer hydrophilic surfaces, favoring the adhesion of cells such as osteoblasts [27]. CA measurements of the water droplets on the HA disc surface showed a significant decrease in HA surface hydrophilicity after RGD physical adsorption. In contrast, the complete chemical immobilization of RGD on the HA surface led to a slight increase in the contact angle, from 61° to 69°, suggesting that hydrophilicity was slightly affected in the RGD bond functionalized HA surface. The low hydrophilicity of the c-RGDHA sample was attributed to -NH₂⁺ terminals, which was in agreement with the results from the Zeta potential assessments [23]. These topographical changes, in combination with surface charge modifications detected by zeta potential (ZP) analysis, suggest that chemical immobilization may create a more stable environment for RGD, potentially enhancing its bioactivity.

Despite these modifications, our cell adhesion assays revealed that the number of pre-osteoblast cells (MC3T3-E1) adhered to RGD-functionalized surfaces did not significantly differ from the untreated HA when cultivated in a serum-free medium. This result is in convergence with previous reports [10,18], where treatment with serum was necessary to identify the effects of RGD in cell adhesion over HA, indicating that serum proteins play a crucial role in mediating cell adhesion on HA surfaces, potentially outcompeting RGD for binding sites and facilitating cell attachment. In contrast, when cultivated in a serum-supplemented medium, chemically immobilized RGD surfaces showed a slight but statistically significant increase in cell adhesion compared to physically adsorbed RGD, although the overall difference was modest. Tatrai et al. [9] demonstrated that cyclic RGD was physically adsorbed using a branched-chain polypeptide, resulting in a more significant electrostatic interaction that accelerated the adipocyte adhesion (AdMSC) in the serum-free medium. The weak binding of RGD to the HA surface may explain the different results of cell adhesion when RGD is physically immobilized on the HA surface. In this case, RGD may be released from the surface because adsorption occurs through the electrostatic interaction mediated by the water molecules chemically bound to the HA surface. On the other hand, the stabilization of RGD on the HA surface by chemical binding aimed to increase the number of adhered cells by offering higher attachment points for adhesion, accelerating the interaction process. The higher cell adhesion on c-RGD/HA confirmed the role of RGD in cell adhesion in the serum-free medium and the need for stabilized RGD onto the biomaterial surface to improve cell–surface interactions.

Uncoated HA, p-RGD/HA, and c-RGD/HA adsorbed the proteins present in the FBS via electrostatic interaction, thus promoting similar cell adhesion in all tested groups. Hydrophilic surfaces, such as HA, favor the adsorption of the adhesive proteins present in FBS by electrostatic interactions, thus promoting cell adhesion [28]. According to the FBS adsorption assays, the p-RGD/HA surface adsorbed the same amount of FBS as HA did, suggesting an RGD displacement by the FBS proteins, as proposed by Sawyer et al. [10] and Hennessy et al. [14]. In the c-RGD/HA sample, the chemical binding of RGD with the HA surface led to a decrease in FBS protein adsorption. However, the amount of proteins still binding to the disc surface (5.7 micrograms/mL) was enough to stimulate cell adhesion, as also observed on the HA and p-RGD surfaces. This result revealed that the simple presence of FBS proteins on the surface might be sufficient to start the effective adhesion process.

Previous studies have reported similar findings, where serum proteins, rich in fibronectin (FN) and vitronectin (VN), preferentially mediate cell adhesion over RGD-functionalized surfaces. By being rich in FN and VN, FBS may activate cell adhesion equally or better than the peptide sequences containing RGD when adsorbed on the HA surfaces [10,17,18], even when compared to the specific sequences of the proteins FN-RGD and VN-RGD [27]. Kilpadi et al. [29] compared the coated CaP with FBS, VN, and FN separately and observed that human mesenchymal stem cells (hMSCs) still preferred HA when covered by FBS, while Saos-2 cells preferred HA with FN or FBS to surfaces with immobilized FN-RGD and VN-RGD segments. RGD segments bind to specific groups of integrins, such as cRGDfK to $\alpha\beta3$ and $\alpha\beta5$, highly expressed by the angiogenic endothelial cells [7]. The MC3T3-E1 pre-osteoblastic cells bind preferentially to the FN and VN proteins through the expressed integrins of $\alpha5\beta1$ and $\alpha\beta3$, which are directly involved in the initial adhesion of the bone cells [27]. Such specificity may answer the preference of MC3T3-E1 for FBS-coated HA surfaces compared to HA that is associated with the RGD tripeptide, as previously described by Mavropoulos et al. [13].

There are still some important considerations about the functionality of RGD that may impair the establishment of comparisons between studies, such as the type of peptides, as well as the concentrations used and the methodology employed, both in the production and characterization of the functionalized surfaces and in the biological evaluation, making it more difficult to reach a more precise conclusion on the subject. In this regard, one of the inherent challenges in this study was determining the precise amount of RGD modification or adsorption and ensuring identical levels across the physical and chemical immobilization methods. The distinct mechanisms underlying physical adsorption and chemical bonding of RGD to the HA surface create intrinsic differences in the way RGD interacts with the material. While fluorescence assays using RGD-FITC were employed to quantify the relative amounts of RGD on the surfaces, and our results indicated similar levels of RGD incorporation by both methods, achieving exact quantitative equivalence is inherently complex. This complexity arises from the different surface chemistries and interaction dynamics involved in each immobilization method. Despite this limitation, our approach provides valuable insights into the functional implications of these differences, particularly in the context of cell adhesion and surface interactions. By focusing on the biological outcomes rather than absolute quantitative equivalence, we highlight the relevance of each method in creating functional biomaterials. The present findings indicate that the physical adsorption of RGD on HA promotes cell adhesion, but the low stability of the peptide on the surface reduces its efficacy. Stabilizing RGD on the HA surface through chemical association may be a good solution if the HA active surface sites remain partially available after functionalization to interact with proteins and growth factors that participate in cell adhesion and proliferation. The results of this study highlight the differential effects of RGD immobilization on the surface morphology and biological performance of hydroxyapatite (HA). Our findings demonstrate that both physical adsorption and chemical bonding of RGD to HA surfaces significantly impact cell adhesion, with chemically immobilized RGD showing enhanced effects, particularly in the presence of serum proteins. This aligns with previous studies, such as those by Durrieu et al. [21] and Balasundaram et al. [22], which

underscore the importance of surface functionalization in promoting osteoblast adhesion and subsequent bone formation. However, our work also reveals that the method of RGD immobilization, whether physical or chemical, introduces variations in surface morphology and cell behavior, which are critical for the design of biomaterials.

Mechanistically, the differences observed in cell adhesion between physically adsorbed and chemically bonded RGD can be attributed to the altered surface chemistry and topography resulting from each immobilization technique. Chemical bonding, as facilitated by cross-linking agents like EDC, creates a more stable and bioactive surface, promoting stronger integrin-mediated cell attachment, as supported by the work of Fujisawa et al. [16] and Sawyer et al. [18]. This enhanced bioactivity is particularly evident in our AFM results, which show increased surface roughness and more uniform peptide distribution in chemically treated samples. These findings suggest that the specific surface interactions facilitated by chemical immobilization are crucial for optimizing cell adhesion and, ultimately, bone regeneration.

The broader implications of these findings suggest that the method of RGD immobilization should be carefully considered when designing future osteoconductive scaffolds. While chemical immobilization offers greater stability and potentially enhanced cell adhesion in serum-free environments, it also alters the surface properties of HA in ways that could reduce its interaction with key serum proteins, potentially limiting its efficacy *in vivo*. On the other hand, physical adsorption maintains more of the native HA surface characteristics but may result in weaker peptide attachment, particularly in the presence of serum. These insights could influence the choice of immobilization method based on the specific clinical application, where stability, bioactivity, and the interaction with serum proteins must be balanced to optimize the scaffold's performance in promoting bone regeneration.

5. Conclusions

This study demonstrated that both physical adsorption and chemical immobilization methods effectively bound RGD peptides to HA surfaces at similar concentrations. However, the immobilization method significantly influenced the surface characteristics and biological performance of the material. In serum-free conditions, chemically immobilized RGD showed enhanced cell adhesion compared to physically adsorbed RGD and untreated surfaces. This improvement is likely due to the more stable and bioactive surface created by chemical bonding, which also resulted in a smoother topography and modified surface charge. However, in serum-supplemented conditions, the impact of RGD functionalization on cell adhesion was less pronounced, suggesting that serum proteins may play a more crucial role in mediating cell adhesion on HA surfaces than RGD functionalization alone. These findings underscore the importance of carefully selecting the immobilization method for RGD when designing biomaterials for bone regeneration. While chemical immobilization provides greater stability and potentially enhances cell adhesion in environments devoid of serum proteins, it also reduces the material's ability to interact with key serum proteins, which could limit its effectiveness *in vivo*. On the other hand, physical adsorption maintains more of the native HA surface properties but may lead to weaker peptide attachment, particularly in the presence of serum. The choice of immobilization method should thus be tailored to the specific clinical application, balancing stability, bioactivity, and interaction with serum proteins to optimize the scaffold's performance in promoting bone regeneration.

Supplementary Materials: The following supporting information can be downloaded at: <https://www.mdpi.com/article/10.3390/app14177479/s1>, Figure S1: Fourier-transform infrared spectroscopy (FTIR) of hydroxyapatite (HA) with thermal treatment at 1000 °C, with OH⁻ at 3570 and (PO₄)³⁻ bands at 1091, 1044, 959, 632, 601, and 569 cm⁻¹; Figure S2: The X-ray photoelectron spectroscopy (XPS) spectra of the uncoated sample consisted of binding energies of O 1s (532.3, 530.7, and 528.6 eV), Ca 2p_{3/2} (346.7.1 and 344.5 eV), P 2p_{3/2} (132.5 eV), and C 1s (288.3, 286.1, and 284.5 eV); Table S1: Chemical analyses by X-ray fluorescence (XRF).

Author Contributions: Conceptualization, G.G.A. and A.M.R.; methodology, M.L., E.M., G.N.F., M.S.S., A.C., E.L. and J.M.G.; software, M.L., E.M., M.S.S., A.C., G.N.F., E.L. and J.M.G.; validation, A.M.R. and C.F.M.; formal analysis, A.M.R., T.R., A.P. and C.F.M.; investigation, A.M.R., T.R. and C.F.M.; resources, G.G.A. and A.M.R.; data curation, M.L., E.M., G.N.F., M.S.S., A.C., E.L. and J.M.G.; writing—original draft preparation, M.L., G.G.A. and A.M.R.; writing—review and editing, A.M.R., N.D.P. and T.R.; visualization, T.R., N.D.P. and A.P.; supervision, A.M.R. and G.G.A.; project administration, A.M.R.; funding acquisition, A.M.R. All authors have read and agreed to the published version of the manuscript.

Funding: This research received no external funding.

Institutional Review Board Statement: Not applicable.

Informed Consent Statement: Not applicable.

Data Availability Statement: The original contributions presented in the study are included in the article/supplementary material, and further inquiries can be directed to the corresponding author.

Acknowledgments: Authors would like to acknowledge FAPERJ, CAPES, and CNPq.

Conflicts of Interest: The authors declare no conflicts of interest.

References

1. Fendi, F.; Abdullah, B.; Suryani, S.; Usman, A.N.; Tahir, D. Development and application of hydroxyapatite-based scaffolds for bone tissue regeneration: A systematic literature review. *Bone* **2024**, *183*, 117075. [[CrossRef](#)]
2. Henkel, J.; Woodruff, M.A.; Epari, D.R.; Steck, R.; Glatt, V.; Dickinson, I.C.; Choong, P.F.M.; Schuetz, M.A.; Huttmacher, D.W.; Mason, C.; et al. Bone Regeneration Based on Tissue Engineering Conceptions—A 21st Century Perspective. *Bone Res.* **2013**, *1*, 216–248. [[CrossRef](#)] [[PubMed](#)]
3. Lee, W.-H.; Loo, C.-Y.; Rohanzadeh, R. A review of chemical surface modification of bioceramics: Effects on protein adsorption and cellular response. *Colloids Surf. B Biointerfaces* **2014**, *122*, 823–834. [[CrossRef](#)]
4. Glaeser, R.M. Proteins, Interfaces, and Cryo-Em Grids. *Curr. Opin. Colloid Interface Sci.* **2018**, *34*, 1–8. [[CrossRef](#)] [[PubMed](#)]
5. Kowalski, P.S.; Bhattacharya, C.; Afewerki, S.; Langer, R.S. Smart Biomaterials: Recent Advances and Future Directions. *ACS Biomater. Sci. Eng.* **2018**, *4*, 809–3817. [[CrossRef](#)] [[PubMed](#)]
6. Bellis, S.L. Advantages of RGD peptides for directing cell association with biomaterials. *Biomaterials* **2011**, *32*, 4205–4210. [[CrossRef](#)]
7. Notni, J. RGD Forever!—Past, Present, and Future of a 3-Letter-Code in Radiopharmacy and Life Sciences. *Pharmaceuticals* **2022**, *16*, 56. [[CrossRef](#)]
8. Fricain, J.C.; Pothuau, L.; Durrieu, M.C.; Pallu, S.; Bareille, R.; Renard, M.; Jeanfils, J.; Dard, M.; Amédée, J.; Amedee, J. Effects of cyclic RGD peptide functionalization on the quantitative bone ingrowth process in cellularized biphasic calcium phosphate ceramics. *Key Eng. Mater.* **2005**, *284*, 647–650.
9. Tatrai, P.; Sagi, B.; Szigeti, A.; Szepesi, A.; Szabo, I.; Bosze, S.; Kristof, Z.; Marko, K.; Szakacs, G.; Urban, I.; et al. A novel cyclic RGD-containing peptide polymer improves serum-free adhesion of adipose tissue-derived mesenchymal stem cells to bone implant surfaces. *J. Mater. Sci.-Mater. Med.* **2013**, *24*, 479–488. [[CrossRef](#)] [[PubMed](#)]
10. Sawyer, A.A.; Hennessy, K.M.; Bellis, S.L. The effect of adsorbed serum proteins, RGD and proteoglycan-binding peptides on the adhesion of mesenchymal stem cells to hydroxyapatite. *Biomaterials* **2007**, *28*, 383–392. [[CrossRef](#)]
11. Yang, C.; Cheng, K.; Weng, W.; Yang, C. Immobilization of RGD peptide on HA coating through a chemical bonding approach. *J. Mater. Sci. Mater. Med.* **2009**, *20*, 2349–2352. [[CrossRef](#)] [[PubMed](#)]
12. Pothuau, L.; Fricain, J.-C.C.; Pallu, S.; Bareille, R.; Renard, M.; Durrieu, M.-C.C.; Dard, M.; Vernizeau, M.; Amedee, J.; Amédée, J. Mathematical modelling of the distribution of newly formed bone in bone tissue engineering. *Biomaterials* **2005**, *26*, 6788–6797. [[CrossRef](#)]
13. Mavropoulos, E.; Hausen, M.; Costa, A.M.; Alves, G.; Mello, A.; Ospina, C.A.; Mir, M.; Granjeiro, J.M.; Rossi, A.M. The impact of the RGD peptide on osteoblast adhesion and spreading on zinc-substituted hydroxyapatite surface. *J. Mater. Sci.-Mater. Med.* **2013**, *24*, 1271–1283. [[CrossRef](#)] [[PubMed](#)]
14. Hennessy, K.M.; Clem, W.C.; Phipps, M.C.; Sawyer, A.A.; Shaikh, F.M.; Bellis, S.L. The effect of RGD peptides on osseointegration of hydroxyapatite biomaterials. *Biomaterials* **2008**, *29*, 3075–3083. [[CrossRef](#)]
15. Bitschnau, A.; Alt, V.; Bohner, F.; Heerich, K.E.; Margesin, E.; Hartmann, S.; Sewing, A.; Meyer, C.; Wenisch, S.; Schnettler, R. Comparison of new bone formation, implant integration, and biocompatibility between RGD-hydroxyapatite and pure hydroxyapatite coating for cementless joint prostheses—an experimental study in rabbits. *J. Biomed. Mater. Res. Part B Appl. Biomater.* **2009**, *88*, 66–74. [[CrossRef](#)]
16. Fujisawa, R.; Mizuno, M.; Nodasaka, Y.; Yoshinori, K. Attachment of osteoblastic cells to hydroxyapatite crystals by a synthetic peptide (Glu7-Pro-Arg-Gly-Asp-Thr) containing two functional sequences of bone sialoprotein. *Matrix Biol.* **1997**, *16*, 21–28. [[CrossRef](#)] [[PubMed](#)]

17. Le Guillou-Buffello, D.; Bareille, R.; Gindre, M.; Sewing, A.; Laugier, P.; Amedee, J.; Amédée, J. Additive effect of RGD coating to functionalized titanium surfaces on human osteoprogenitor cell adhesion and spreading. *Tissue Eng. Part A* **2008**, *14*, 1445–1455. [[CrossRef](#)] [[PubMed](#)]
18. Sawyer, A.A.; Hennessy, K.M.; Bellis, S.L. Regulation of mesenchymal stem cell attachment and spreading on hydroxyapatite by RGD peptides and adsorbed serum proteins. *Biomaterials* **2005**, *26*, 1467–1475. [[CrossRef](#)] [[PubMed](#)]
19. Eanes, E.D.; Gillessen, I.H.; Posner, A.S. Intermediate States in the Precipitation of Hydroxyapatite. *Nature* **1965**, *208*, 365–367. [[CrossRef](#)]
20. Moulder, J.F.; Stickle, W.F.; Sobol, P.E.; Bomben, K.D. *Handbook of X-ray Photoelectron Spectroscopy: A Reference Book of Standard Spectra for Identification and Interpretation of XPS Data; Surface and Interface Analysis*; Perkin-Elmer Corporation: Waltham, MA, USA, 1992; p. 261. ISBN 9780962702624.
21. Durrieu, M.C.; Pallu, S.; Guillemot, F.; Bareille, R.; Ame, J.; Baquey, C.H.; Tissulaire, Â.; Saignat, Â.; Inserm, U.; Labruge, C.; et al. Grafting RGD containing peptides onto hydroxyapatite to promote osteoblastic cells adhesion. *J. Mater. Sci. Mater. Med.* **2004**, *15*, 779–786. [[CrossRef](#)]
22. Balasundaram, G.; Sato, M.; Webster, T.J. Using hydroxyapatite nanoparticles and decreased crystallinity to promote osteoblast adhesion similar to functionalizing with RGD. *Biomaterials* **2006**, *27*, 2798–2805. [[CrossRef](#)] [[PubMed](#)]
23. López, E.O.; Rossi, A.L.; Archanjo, B.S.; Ospina, R.O.; Mello, A.; Rossi, A.M. Crystalline nano-coatings of fluorine-substituted hydroxyapatite produced by magnetron sputtering with high plasma confinement. *Surf. Coat. Technol.* **2015**, *264*, 163–174. [[CrossRef](#)]
24. Sun, C.C.; Qu, X.J.; Gao, Z.H. Arginine-Glycine-Aspartate-Binding Integrins as Therapeutic and Diagnostic Targets. *Am. J. Ther.* **2016**, *23*, e198–e207. [[CrossRef](#)] [[PubMed](#)]
25. Rabe, M.; Verdes, D.; Seeger, S. Understanding protein adsorption phenomena at solid surfaces. *Adv. Colloid Interface Sci.* **2011**, *162*, 87–106. [[CrossRef](#)] [[PubMed](#)]
26. Rouahi, M.; Gallet, O.; Champion, E.; Dentzer, J.; Hardouin, P.; Anselme, K. Influence of hydroxyapatite microstructure on human bone cell response. *J. Biomed. Mater. Res. A* **2006**, *78*, 222–235. [[CrossRef](#)] [[PubMed](#)]
27. Felgueiras, H.P.; Evans, M.D.M.; Migonney, V. Contribution of fibronectin and vitronectin to the adhesion and morphology of MC3T3-E1 osteoblastic cells to poly(NaSS) grafted Ti6Al4V. *Acta Biomater.* **2015**, *28*, 225–233. [[CrossRef](#)]
28. Liu, Z.; Zhou, Y.; Kimura, R.; Tagaya, M. Analytical investigation of nano-bio interfacial protein mediation for fibroblast adhesion on hydroxyapatite nanoparticles. *Phys. Chem. Chem. Phys.* **2023**, *25*, 4025–4034. [[CrossRef](#)]
29. Kilpadi, K.L.; Sawyer, A.A.; Prince, C.W.; Chang, P.-L.L.; Bellis, S.L. Primary human marrow stromal cells and Saos-2 osteosarcoma cells use different mechanisms to adhere to hydroxylapatite. *J. Biomed. Mater. Res.—Part A* **2004**, *68*, 273–285. [[CrossRef](#)]

Disclaimer/Publisher’s Note: The statements, opinions and data contained in all publications are solely those of the individual author(s) and contributor(s) and not of MDPI and/or the editor(s). MDPI and/or the editor(s) disclaim responsibility for any injury to people or property resulting from any ideas, methods, instructions or products referred to in the content.